Jour. Fac. Sci., Hokkaido Univ., Ser. IV,
vol. 23, no. 2, Aug., 1992. pp. 255-280

# TEXTURE, CHEMICAL COMPOSITION AND GENESIS OF SCHREIBERSITE IN IRON METEORITE

*by*

**Masahide Yoshikawa* and Hiroharu Matsueda**

(with 13 text-figures, 9 tables and 3 plates)

*Abstract*

Thirteen iron meteorites composed of Hexahedrite, Octahedrite and Ataxite were investigated to estimate their cooling history and origin. They are mainly composed of Fe-Ni metals (kamacite and taenite) with smaller amounts of schreibersite $(Fe, Ni)_3P$ and sulfides (troilite and sphalerite).

Schreibersite occurs an idiomorphic and xenomorphic crystals and its mode of occurrence is variable in iron meteorites. Xenomorphic schreibersite is subdivided into 6 types on the basis of their textures and relationships with coexisting minerals. Chemical composition of schreibersite varies from 20 to 40 atom. % Ni with textural types among some iron meteorites with different bulk chemical compositions and even in the same meteorite (*e. g.* Canyon Diablo), while it does not vary so clear with textural types in ALH-77263.

Schreibersite seems to maintain a local equilibrium with coexisting metal phases. Based on the Fe-Ni-P phase diagram, it is estimated that xenomorphic and coarse-grained schreibersite in Y-75031 and in DRPA 78007 were crystallized from stability field of taenite and schreibersite at about 800℃ under rapid diffusion conditions. Cooling rates within the parent bodies are calculated by using the diffusion rate of Ni between schreibersite and kamacite as follows; Canyon Diablo: $1.1\times10^6$, Odessa: $1.7\times10^6$, North Chile: $2.3\times10^6$, ALH-77263: $8.7\times10^7$ (year/℃). It is considered that ALH-77263 had been cooled keeping more equilibrated state with slower cooling rate than Canyon Diablo.

Variable textures and chemical compositions of schreibersite suggest that it had been maintained a local equilibrium with kamacite. Estimated temperatures at which the reaction mostly completed among metals and sulfide tend to show higher value in unequilibrated iron meteorites than equilibrated ones. It is inferred that unequilibrated iron meteorites had been rapidly cooled, but equilibrated ones slowly to maintain diffusion under the lower temperatures.

## Introduction

Meteorite is classified into three types which are stony, stony-iron and iron meteorites. Iron meteorite is mainly composed of kamacite $\alpha$-(Fe, Ni) and taenite $\gamma$-(Fe, Ni). It also contains small amounts of schreibersite $(Fe, Ni)_3P$, troilite FeS, sphalerite ZnS and some other minerals. Iron meteorite is classified into three types, Hexahedrite, Octahedrite and Ataxite on the basis of textures (Bushwald, 1975). Text-fig. 1 is a polished surface of the Harlowton iron meteorite etched by nitric acid. It represents a typical Widmanstätten structure controlled by bulk Ni content.

---

Contribution from the Department of Geology and Mineralogy, Faculty of Science, Hokkaido University, No. 2070

* Sumitomo Metal Industries, Co. Ltd., Kashima, Ibaragi, 314, Japan

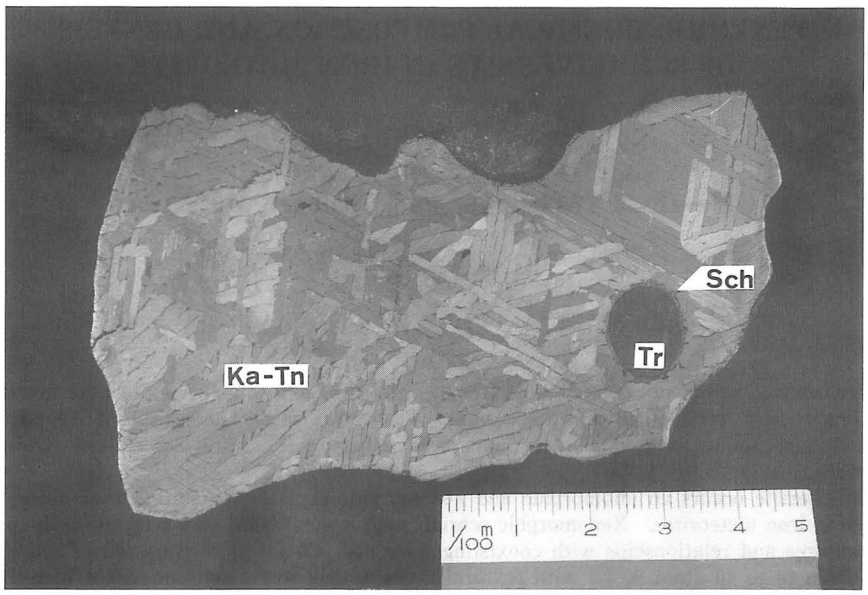


**Text-fig. 1** Polished and etched surface of Harlowton iron meteorite, showing representative Widmanstätten structure composed of kamacite (Ka) and taenite (Tn) with globular troilite (Tr) surrounded by schreibersite (Sch).

In this study eight iron meteorites from Antarctica and five from other localities, were used for laboratory works. It is infered that iron meteorite is a substance from the core of parent body and is released with a destruction of parent body. So it is expected that iron meteorite keeps not only the informations of chemical compositions and mineral assemblages of planetary core but also thermal and/or pressure history. Further, Kelly and Larimer (1977) suggests that variation of the types of iron meteorite reflects the formation process of planet which combines a planetesimal with a collision.

Iron meteorites have been studied especially for metal phases in detall, but discussion on the genesis of schreibersite is quite few. Therefore, special attentions are paid for the schreibersite with reference to their textures, and modal and chemical compositions in this study. Further, the textures and the chemical compositions of metal phases, troilite and sphalerite are also examined in relation to schreibersite. Based on these studies, cooling history and origin of iron meteorites are estimated.

## Experiments

Samples

Thirteen iron meteorites used for this study are listed in Table 1 with chemical classification by Wasson (1974) and with textural one. In these specimens, ALH-77283, ALH-77263, DRPA 78007, Y-790517, Y-790724, ALH-78252, Y-75031

**Table 1** Chemical compositions of investigated samples. Data after Bushwald (1975), Fisher *et al.* (1985) and Nagata *et al.* (1978 & 1980), Graham *et al.* (1983, 1984 & 1986).

| Name | Group | Class | Composition(wt. %) | | | | |
|---|---|---|---|---|---|---|---|
| | | | Ni | Co | P | S | C |
| Canyon Diablo | I A | Og | 7.10 | 0.46 | 0.26 | 1.00 | 1.00 |
| ALH-77283 | I A | Og | 7.33 | 0.50 | 0.22 | | |
| Odessa | I A | Og | 7.35 | 0.48 | 0.25 | 0.50 | 0.20 |
| ALH-77263 | I A | Og | 6.78 | 0.47 | 0.20 | | |
| Harlowton | I A | Om | 8.27 | 0.44 | 0.17 | | |
| North Chile | II A | H | 5.59 | 0.48 | 0.30 | | |
| DRPA 78007 | II B | Ogg | 7.30 | 0.38 | 0.75 | | |
| Y-790517 | III A | Om | 7.42 | 0.58 | 0.41 | | |
| Y-790724 | III A | Om | 7.47 | 0.45 | 0.12 | | |
| Boxhole | III A | Om | 7.67 | 0.49 | 0.11 | 0.05 | |
| ALH-78252 | IV A | Om | 9.33 | 0.43 | 0.17 | | |
| Y-75031 | ? | Opl | 15.30 | 0.76 | 1.00 | | |
| Y-791694 | ? | D | 35.50 | 0.60 | 0.15 | | |

H ; Hexahedrite, Ogg ; Coarsest Octahedrite, Og ; Coarse Octahedrite, Om ; Medium Octahedrite, Opl ; Plessitic Octahedrite, D ; Ataxite.

and Y-791694 are iron meteorites from Antarctica. Among them ALH, DRPA and Y mean the collected places respectively such as Allan Hills, Derick Peak and Yamato Mountains, and the first two figures are the year of collection followed with order of finding. These Antarctic meteorite samples are lent for the investigation from the National Institute of Polar Research, Japan.

Canyon Diablo, Odessa, Harlowton, North Chile and Boxhole are non-Antarctic iron meteorites. Odessa and Boxhole are offered for this study from Akita University, and Harlowton is from the Mineral Museum of Montana College of Mineral Science and Technology.

In Table 1, bulk chemical compositions of iron meteorites are also shown in each specimen. Bulk Ni contents varies from 5.59 weight % (North Chile) to 35.5 weight % (Y-791694) in these meteorites. They cover all kind of iron meteorites including Hexahedrite, Octahedrite and Ataxite. Bulk P content varies from 0.11 weight % (Boxhole) to 1.00 weight % (Y-75031) among them.

## Analytical procedures

Samples were polished by #1000, #2000, and #3000 of alumina powders and also by 1 $\mu$m and 0.25 $\mu$m of diamond one. A part of polished sample was etched by picric acid (4%) or nitric acid (1%) for the textural observation under the reflected-light microscope. Scheribersite belongs to tetragonal system and shows extremely strong anisotropism under the microscope.

Chemical compositions of individual minerals were determined by electron

probe microanalyzer (EPMA). Analytical conditions are as follows;

Machine : JEOL JCMA-733
X-ray take off angle : 40 degrees
Accelerating voltage : 20 kV
Sample current : $1.8\times10^{-8}$ A
Correction methods : ZAF program distributed by JEOL (Hirata, 1985)
Used characteristic X-rays and standard materials:
Fe K$\alpha$, Ni K$\alpha$, Co K$\alpha$, Cr K$\alpha$ ; metals
Zn K$\alpha$ ; ZnS(syn.)
S K$\alpha$ ; ZnS(syn.) for sphalerite
$FeS_2$(syn.) for others
P K$\alpha$ ; GaP(syn.)

Modal proportions of idiomorphic schreibersite measured for 1.3 mm×0.9 mm square area were obtained by a digital image processor with personal computer, TV camera and an image digitizing board (Fujikawa and Matsueda, 1991). Equivalent radii were also measured by using the same system. On the other hand, modal proportions of xenomorphic schreibersite were determined by a weighing method of sketched paper for the whole sample and schreibersite, because xenomorphic schreibersite is too big in grain size to determine the modal proportion by digital image processing.

## Textures and chemical compositions of schreibersite

Classification of textures

Schreibersite $(Fe, Ni)_3P$ occurs commonly in iron meteorites. It shows both xenomorphic and idiomorphic textures. The former are subdivided into five types ((a) through (c), (e) and (f)) on the basis of the relationships with coexisting minerals. The latter are types (d) and (g).

(a) *Xenomorphic and coarse-grained screibersite coexisting with kamacite*

Schreibersite of this type coexists with kamacite and occurs at the boundary between kamacite grains. It shows xenomorphic texture and is 100 $\mu$m to 1 mm in size (Plate 1-a). Ni contents of this type is about 20 atomic %, and it is lower than another types of schreibersite.

(b) *Xenomorphic schreibersite in the extension of taenite with a Widmanstätten structure*

This type of schreibersite occurs as straight line with taenite. It seems to occupy the extended position of taenite showing Widmanstätten strucrure (Plate 1-b). The Ni content of schreibersite is about 38 atomic % in this type.

(c) *Xenomorphic and fine-grained schreibersite coexisting with kamacite*

This type of schreibersite coexists with kamacite showing xenomorphic and

**Table 2** Classification of textural types of schreibersite in iron meteorites.

| Texture | Name and Group | | | | | | | | | | | | |
|---|---|---|---|---|---|---|---|---|---|---|---|---|---|
| | Canyon Diablo | ALH-77283 | Odessa | ALH-77263 | Harlowton | North Chile | DRPA 78007 | Y-790517 | Y-790724 | Boxhole | ALH-78252 | Y-75031 | Y-791694 |
| | IA | IA | IA | IA | IA | IIA | IIB | IIIA | IIIA | IIIA | IVA | ? | ? |
| a | | | | | | | + | | | | | +++ | |
| b | | | − | − | | | − | | | | | | |
| c | ++ | + | + | + | + | + | | + | | | + | | |
| d | + | | + | + | ++ | ++ | ++ | | | | | | |
| e | − | − | − | − | − | | − | | − | − | | ++ | + |
| f | − | + | | | − | + | | | | | − | | |
| g | | | | | | − | | | | | | | |

+++ very abundant, ++ abundant, + common, − rare.

a: xenomorphic and coarse-grained schreibersite coexisting with kamacite, b: xenomorphic schreibersite in the extension of taenite with a Widmanstätten structure, c: xenomorphic and fine-grained schreibersite coexitsing with kamacite, d: idiomorphic schreibersite coexisting with kamacite, e: xenomorphic schreibersite coexisting with plessite, f: xenomorphic schreibersite coexisting with troilite, sphalerite or cohenite, g: platy schreibersite.

string in shape. It occurs at the grain boundary of kamacites and its grain size is smaller than the type (a) of schreibersite (Plate 2-c). Ni content of this type is about 30 atomic % and is different from type (a).

(d) *Idiomorphic schreibersite coexisting with kamacite*

This type of schreibersite shows idiomorphic in shape which is called rhabdite. The tetragonal prismatic crystals are dispersed in kamacite with 10 $\mu$m in grain size (Plate 2-d).

(e) *Xenomorphic schreibersite coexisting with plessite*

This type of schreibersite occurs as mixture with fine-grained kamacite and taenite showing plessite. Its grain size is about 10 $\mu$m (Plate 3-e).

(f) *Xenomorphic schreibersite coexisting with troilite, sphalerite or cohenite*

This type of schreibersite occurs at the rim of troilite (Plate 3-f), sphalerite or cohenite.

The idiomorphic schreibersite commonly occurs as elongated thin plate in Hexahedrite (Plate 3-g) and named as follows in this paper.

(g) *Platy schreibersite.*

Modal proportion

The mode of occurrence of schreibersite texture is compiled in Table 2. Some specimen contain various types of schreibersite within one specimen and others has only single type.

The highest value of modal proprtion of schreibersite in Y-75031 (Table 3) reflects the high bulk P content. Relative amount of types (c) and (d) differs with specimen, for example, Canyon Diablo and North Chile.

Modal proportion of idiomorphic schreibersite varies among different kamacite grains even in an iron meteorite. Text-fig. 2 shows a modal proportion of idiomorphic schreibersite hosted in each kamacite grain of Canyon Diablo. Modal proportions of idiomorphic schreibersite change from 0.13% to 2.83%. Text-fig. 3 indicates a relationship between modal proportion and equivalent radius of idiomorphic schreibersite for the same sample in Text-fig. 2. As shown in the Text-fig. 3, the finer grain size of schreibersite seems to correspond with lower modal proportion.

**Table 3** Modal proportions of different types of schreibersite. Textural types a to g are the same as in Table 2.

| texture / name | a | b | c | d | e | f | g |
|---|---|---|---|---|---|---|---|
| Canyon Diablo | | | 1.0 | 0.8 | tr. | tr. | |
| ALH-77263 | | 0.1 | 0.7 | 0.7 | tr. | | |
| Harlowton | | | 0.6 | 1.1 | tr. | tr. | |
| North Chile | | | 0.3 | 2.2 | | 0.8 | tr. |
| DRPA 78007 | 0.8 | 0.1 | | 1.5 | tr. | | |
| Y-75031 | 7.8 | | | | 1.3 | | |

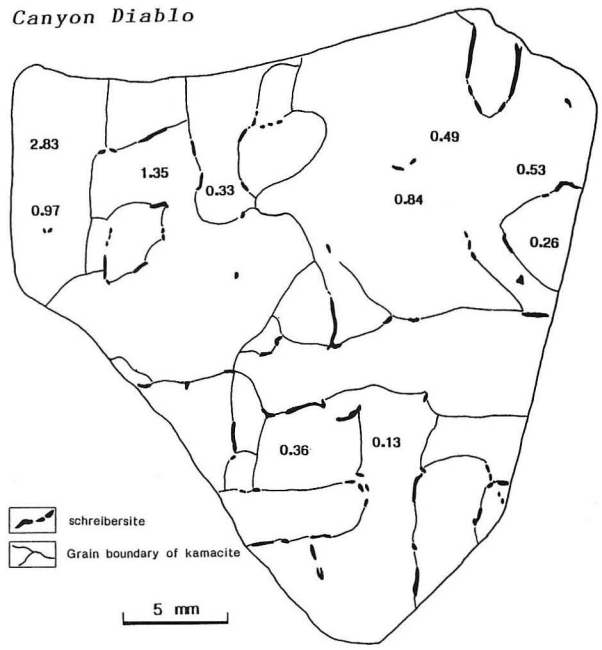


**Text-fig. 2** Modal proportions (0.13~2.83%) of idiomorphic schreibersite in each kamacite grain of Canyon Diablo.

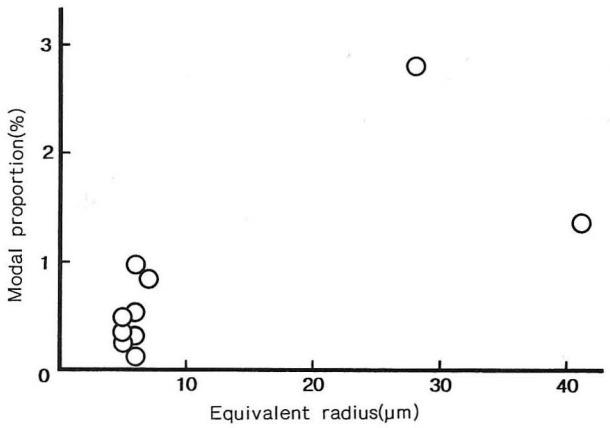


**Text-fig. 3** Relationships between modal proportion and equivalent radius of idiomorphic schreibersite in Canyon Diablo.

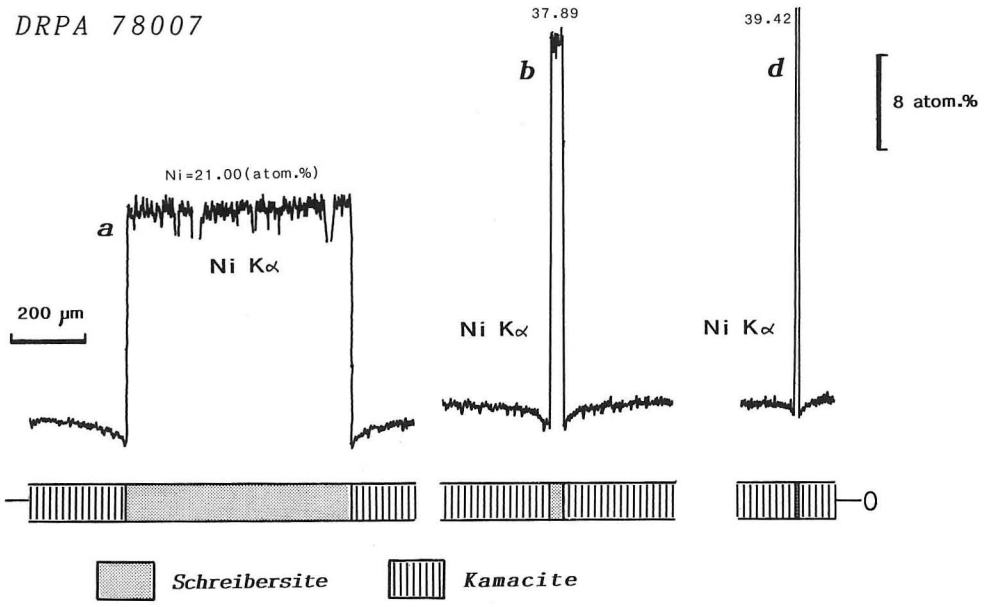


**Text-fig. 4** Line profiles of Ni K$\alpha$ crossing schreibersite and kamacite of types a, b, and d in DRPA 78007.

Chemical compositions

Text-fig. 4 shows Ni K$\alpha$ line profiles of EPMA crossing schreibersite and kamacite of DRPA 78007 for the type (a), (b) and (d). Ni contents in each type of schreibersite are as follows; Type (a)=21.00 atomic %, Type (b)=37.89 atomic %, Type (d)=39.42 atomic %. Considering these data, Ni contents are varies among the different textural types of schreibersite, in which idiomorphic schreibersite shows higher Ni content than others. Ni contents of schreibersite is almost homogeneous in a single grain of all specimen investigated.

Ni/Fe ratio of schreibersite varies not only with specimens but also with grains of different texture in the same specimen. It is high in Harlowton and Canyon Diablo (Text-figs. 5 & 6). Within a specimen it changes regularly with its texture in DRPA 78007 and probably in Y-75301. The ratios in Canyon Diablo Harlowton and in North Chile have narrower range of variation. It has very narrow range in ALH-77263.

## Metal and sulfide phases associated with schreibersite

Fe-Ni metals

Iron meteorite often shows a Widmanatätten structure, a kind of exsolution texture in which kamacite in crystallized along with (111) plane of taenite. Kamacite often shows a mosaic texture by etching test with picric acid or nitric

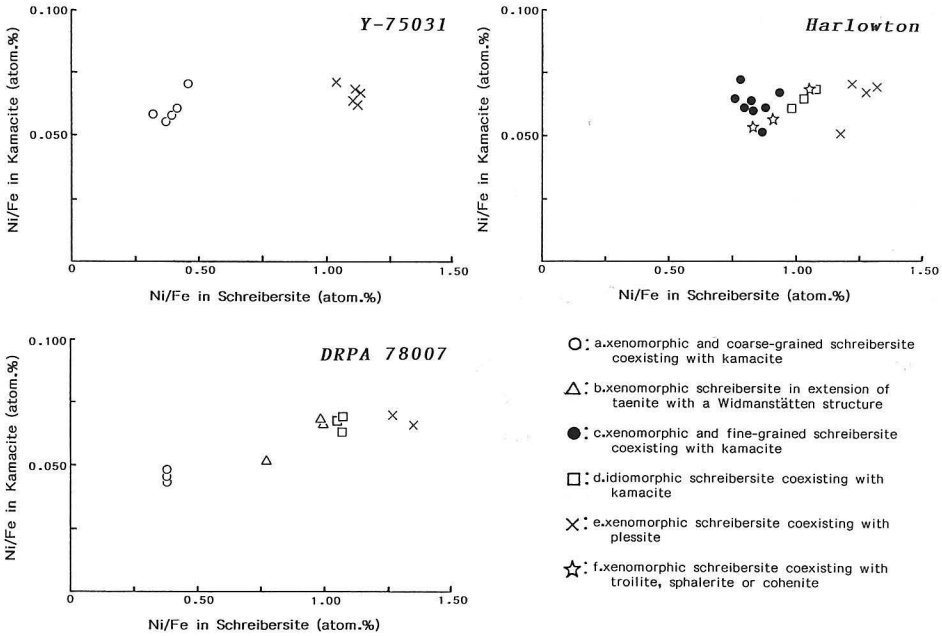


**Text-fig. 5** Relationships of Ni partition between schreibersite and kamacite in Y-75031, DRPA 78007 and Harlowton.

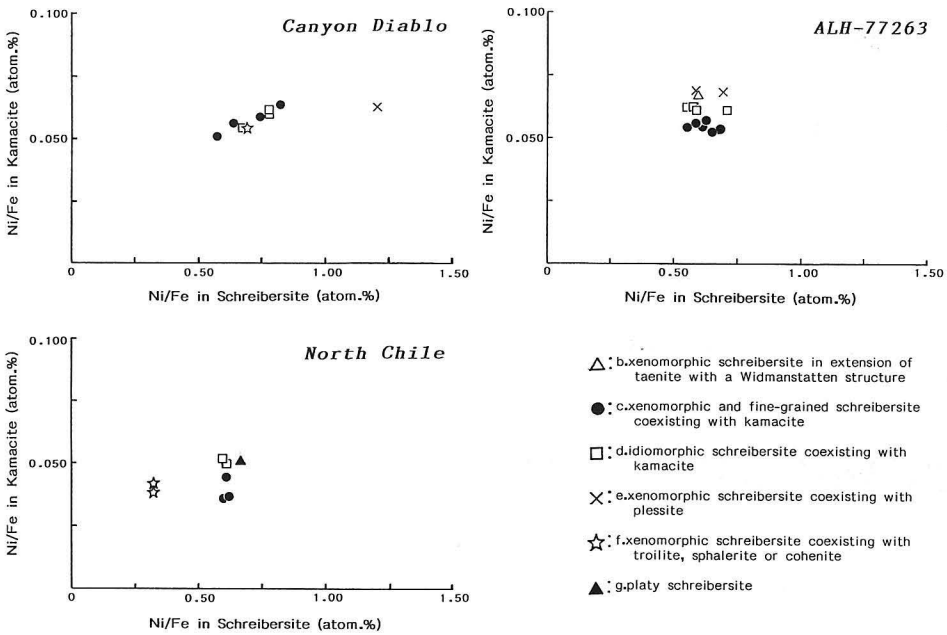


**Text-fig. 6** Relationships of Ni partition between schreibersite and kamacite in Canyon Diblo, North Chile and ALH-77263.

acid. Grain boundaries are more easily etched and the etching degree varies on grain by grain. The degree seems to depend on crystal orientations because the mosaic pattern are also observed in backscattered electron image as a result of channeling effect (Reed, 1975 : pp. 69-71).

Size of grains composing mosaic aggregate varies approximately from 10 to 100 $\mu$m in the meteorite specimens used in this study. Canyon Diablo shows a coarse-grained mosaic texture, in which schreibersite is crystallized mostly along the grain boundaries of kamacites, while a few schreibersite is crystallized in kamacite grain. DRPA 78007 also shows similar mode of occurrence of kamacite and schreibersite. However, this texture in Y-790724 is smaller in grain size (10 $\mu$m in order) than in both of Canyon Diablo and DRPA 78007. Xenomorphic schreibersite in Y-790724 dose not occur along the grain boundaries of kamacite. Namely, the features of mosaic texture of kamacite is different among individual iron meteorites.

Ni K$\alpha$ line profiles by EPMA crossing the grain boundary are shown in Text-fig. 7. Clear Ni decrease is observed at the grain boundary in Canyon Diablo and DRPA 78007. But Ni does not decrease at the grain boundary in Y-790724. Meteorites with coarse-grained mosaic texture show a distinct Ni decrease at the grain boundary, while a meteorite with fine-grained mosaic texture does not show the Ni decreasing phenomena. Width of Ni-decreasing zone in about 100 $\mu$m in Canyon Diablo, while it is more than 100 $\mu$m in DRPA 78007. The changes of chemical composition at the kamacite grain boundary are different from each other in iron meteorites.

Equilibrium temperature is estimated from Ni contents of kamacite and taenite

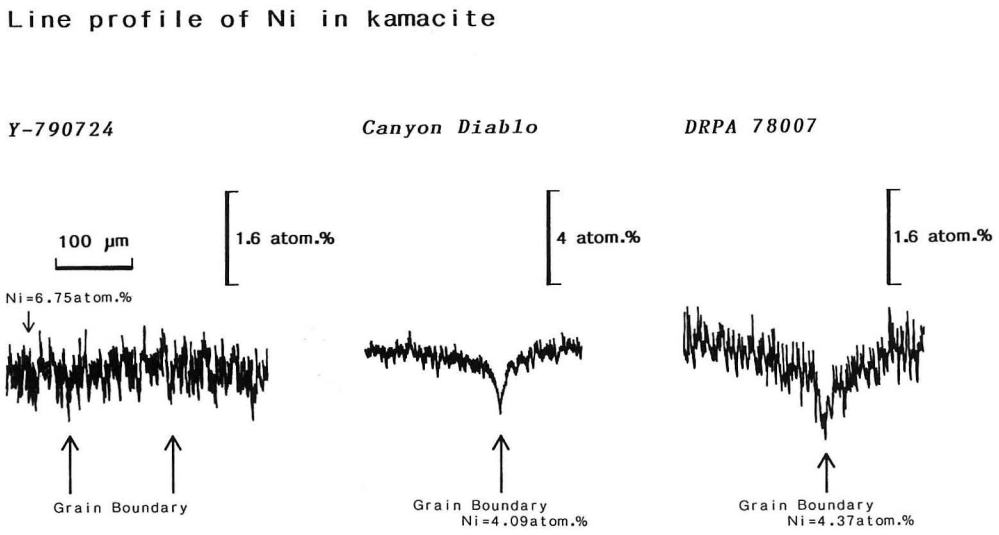


**Text-fig. 7** Ni K$\alpha$ line profiles by EPMA at right angles with grain boundary of kamacite for Y-790724, Canyon Diablo and DRPA 78007.

on the basis of Fe-Ni phase diagram (Goldstein and Ogilvie, 1965). Considering the averaged Ni contents in taenite, estimated equilibrium temperature are as follows; DRPA78007: about 575℃, Harlowton: about 550℃, Y-790724: about 525℃, Equilibrium temperature for kamacite-taenite are different from each other among iron meteorites.

Troilite

Troilite FeS is one of the common sulfide minerals in iron meteorite. It belongs to hexagonal crystal system and shows very strong optical anisotropism. It coexists with kamacite and is often surrounded by schreibersite at its rim. Mosaic texture of troilite is observed by its anisotropism and bireflectance.

Chemical compositions of troilite and coexisting kamacite are shown in Table 4. Fe/S ratio is almost 1 for troilite which contains small amount of Ni (0.01-0.08 atomic %) and Co (0.03-0.06 atomic %).

Bezmen *et al.* (1978) proppsed a method to estimate equilibrium temperature using the Ni partition realtionship between kamacite and troilite. The calculated equilibrium temperatures based on Ni contents of both minerals (Table 4) are as follows: North Chile=364℃, DRPA 78007=471℃, ALH-78252=445℃, Y-75031=499℃. As Ni content of troilite is very small, the above values are not so precise and the statistical errors are shown in Text-fig. 8. In this figure, Y-75031 and DRPA 78007 indicate relatively higher temperature, but North Chile indicates lower one.

**Table 4** Chemical compositions of coexisting troilite (Tr) and kamacite (Ka).

| Name | North Chile | | DRPA78007 | | ALH-78252 | | Y-75031 | |
|---|---|---|---|---|---|---|---|---|
| Min. | Tr | Ka | Tr | Ka | Tr | Ka | Tr | Ka |
| | Weight percent | | | | | | | |
| Fe | 61.42 | 96.83 | 62.80 | 92.86 | 62.62 | 93.98 | 62.58 | 92.19 |
| Ni | 0.01 | 3.93 | 0.07 | 6.55 | 0.07 | 7.21 | 0.10 | 6.65 |
| Co | 0.06 | 0.62 | 0.06 | 0.53 | 0.04 | 0.51 | 0.08 | 0.87 |
| P | 0.00 | 0.06 | 0.00 | 0.03 | 0.00 | 0.10 | 0.01 | 0.11 |
| S | 36.71 | 0.00 | 35.88 | 0.01 | 35.91 | 0.00 | 36.75 | 0.00 |
| Cr | 0.13 | 0.00 | 0.26 | 0.00 | 0.13 | 0.00 | 0.02 | 0.00 |
| Total | 98.33 | 101.44 | 99.07 | 99.98 | 98.77 | 101.80 | 99.54 | 99.82 |
| | Atomic percent | | | | | | | |
| Fe | 48.90 | 95.61 | 49.95 | 93.19 | 49.90 | 92.58 | 49.35 | 92.63 |
| Ni | 0.01 | 3.69 | 0.06 | 6.25 | 0.05 | 6.76 | 0.08 | 6.36 |
| Co | 0.04 | 0.58 | 0.05 | 0.50 | 0.03 | 0.48 | 0.06 | 0.83 |
| P | 0.00 | 0.11 | 0.00 | 0.06 | 0.00 | 0.18 | 0.02 | 0.19 |
| S | 50.92 | 0.00 | 49.72 | 0.01 | 49.86 | 0.00 | 50.48 | 0.00 |
| Cr | 0.11 | 0.00 | 0.22 | 0.00 | 0.11 | 0.00 | 0.02 | 0.00 |
| Total | 100.00 | 100.00 | 100.00 | 100.00 | 100.00 | 100.00 | 100.00 | 100.00 |

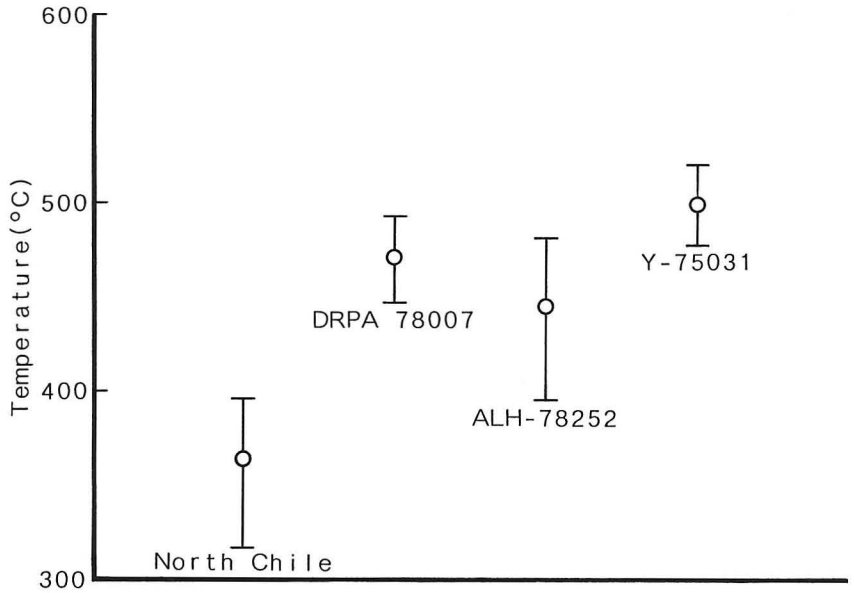


**Text-fig. 8** Equilibrium temperatures estimated from troilite-kamacite paragenesis in iron meteorites.

Sphalerite

Sphalerite commonly occurs in IA type (Wasson, 1979) of iron meteorite (Buchwald, 1975). It coexists with kamacite, and in surrounded by schreibersite at its rim. In this study, the only one grain of sphalerite is found in both Harlowton and Odessa but four grains in Canyon Diablo. Grain sizes of them are ranged from 30 to 130 $\mu$m.

Chemical compositions of sphalerite and coexisting kamacite in Harlowton and Odessa are shown in Table 5. FeS content of sphalerite varies among iron meteorites studied. It is 31.64 mole % in Harlowton, while 12.81 mole % in Odessa.

Chemical compositions of sphalerite and kamacite in Canyon Diablo is shown in Table 6. Analyzed FeS contents for four sphalerite grains are 3.98, 6.80, 14.94, 15.89 mole %, respectively. Individual grain is not so heterogeneous in composition as observed by the backscattered electron image. They occur in different kamacite grains with different FeS content. Fe content of kamacite change from 92.93 to 94.63 atomic % with increasing of FeS content in coexisting sphalerite.

Text-fig. 9. represents Ni K$\alpha$ line profiles (EPMA) for sphalerites in Canyon Diablo. It contains 14.94 mole % FeS in sphalerite(A) and 6.80 mole % FeS in sphalerite(B). Schreibersite occurs at the rim of sphalerite(A). The line profile indicates that Ni content of kamacite coexisting with high FeS sphalerite(A) gradually decreases toward the kamacite-sphalerite grain boundary, namely Fe content of kamacite increases toward the grain boundary. On the other hand, sharp change of Ni content is observed in coexisting kamacite at the grain boundary with

**Table 5** Chemical compositions of coexisting sphalerite (Sph) and kamacite (Ka) in Harlowton and Odessa.

| Name | Harlowton | | Odessa | |
|---|---|---|---|---|
| Min. | Sph | Ka | Sph | Ka |
| | Weight percent | | | |
| Zn | 47.40 | 0.00 | 59.72 | 0.00 |
| Fe | 18.77 | 92.96 | 7.51 | 93.32 |
| Co | 0.04 | 0.63 | 0.01 | 0.60 |
| Ni | 0.01 | 5.94 | 0.08 | 6.44 |
| S | 34.14 | 0.01 | 33.57 | 0.00 |
| P | 0.00 | 0.05 | 0.00 | 0.04 |
| Total | 100.36 | 99.59 | 100.89 | 100.40 |
| | Atomic percent | | | |
| Zn | 34.09 | 0.00 | 43.57 | 0.00 |
| Fe | 15.80 | 93.62 | 6.41 | 93.24 |
| Co | 0.03 | 0.60 | 0.01 | 0.56 |
| Ni | 0.01 | 5.69 | 0.07 | 6.12 |
| S | 50.07 | 0.01 | 49.94 | 0.00 |
| P | 0.00 | 0.09 | 0.01 | 0.08 |
| Total | 100.00 | 100.00 | 100.00 | 100.00 |
| FeS mol. % | 31.64 | | 12.81 | |

**Table 6** Chemical compositions of coexisting sphalerite (Sph) and kamacite (Ka) in Canyon Diablo.

| Point No. | 14-16 | | 18-19 | | 4-7 | | 1-3 | |
|---|---|---|---|---|---|---|---|---|
| Min. | Sph | Ka | Sph | Ka | Sph | Ka | Sph | Ka |
| | Weight percent | | | | | | | |
| Zn | 57.71 | 0.00 | 64.53 | 0.04 | 57.75 | 0.00 | 65.80 | 0.00 |
| Fe | 8.68 | 94.01 | 4.03 | 93.46 | 9.32 | 94.39 | 2.34 | 93.09 |
| Co | 0.02 | 0.65 | 0.01 | 0.55 | 0.00 | 0.64 | 0.00 | 0.54 |
| Ni | 0.08 | 5.20 | 0.11 | 6.70 | 0.02 | 4.88 | 0.09 | 6.68 |
| S | 33.13 | 0.00 | 33.82 | 0.00 | 33.85 | 0.00 | 33.04 | 0.01 |
| P | 0.01 | 0.05 | 0.00 | 0.08 | 0.01 | 0.05 | 0.00 | 0.10 |
| Total | 99.63 | 99.91 | 102.50 | 100.83 | 100.95 | 99.96 | 101.27 | 100.42 |
| | Atomic percent | | | | | | | |
| Zn | 42.57 | 0.00 | 46.65 | 0.04 | 41.91 | 0.00 | 48.38 | 0.00 |
| Fe | 7.49 | 94.33 | 3.41 | 92.97 | 7.92 | 94.63 | 2.01 | 92.93 |
| Co | 0.02 | 0.62 | 0.01 | 0.51 | 0.00 | 0.61 | 0.00 | 0.51 |
| Ni | 0.07 | 4.97 | 0.09 | 6.34 | 0.02 | 4.65 | 0.07 | 6.34 |
| S | 49.83 | 0.00 | 49.85 | 0.00 | 50.09 | 0.00 | 49.54 | 0.03 |
| P | 0.02 | 0.09 | 0.00 | 0.14 | 0.01 | 0.10 | 0.00 | 0.19 |
| Total | 100.00 | 100.00 | 100.00 | 100.00 | 100.00 | 100.00 | 100.00 | 100.00 |
| Fes mol. % | 14.94 | | 6.80 | | 15.89 | | 3.98 | |

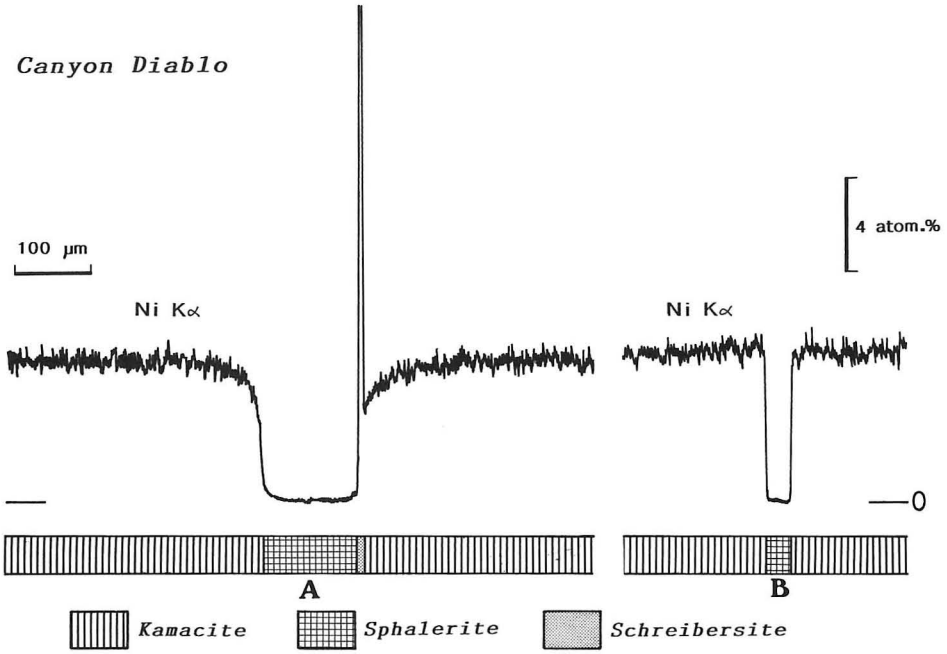


**Text-fig. 9** Ni K$\alpha$ line profiles by EPMA crossing sphalerite and kamacite in Canyon Diablo.

low FeS sphalerite(B).

## Discussion

Genesis of schreibersite

*Formation process*

Thirteen iron meteorites used in this study are classified into two groups, represented by DRPA 78007 and Canyon Diablo, on the basis of the characteristics of schreibersite and accessary phases. Schreibersite varies widely both in chemical composition and texture in the former, while it dose not so much in the latter. Text-fig. 10 shows two sections at differnt Ni contents in the Fe-Ni-P system for iron meteorites on the basis of Doan and Goldstein (1979) and Roming and Goldstein (1980). In this figure, $\alpha$, $\gamma$ and Ph means kamacite, taenite and schreibersite (phosphide), respectively. In DRPA 78007 the arrow indicates a cooling along with 0.75% bulk P in content. It enters a $\gamma$+Ph field at about 875℃ where schreibersite crystallizes at first. After initial crystallization of schreibersite, it will be entered $\alpha$+ph field through $\alpha+\gamma$+Ph field in progress of the meteorite cooling.

Various kinds of schreibersite with different texture and chemical composition are recognized from DRPA 78007 in this study. So it is infered that these different schreibersites have been crystallized in different temperatures where the phosphide can crystallize in cooling process of the meteorite. It might be maintained the

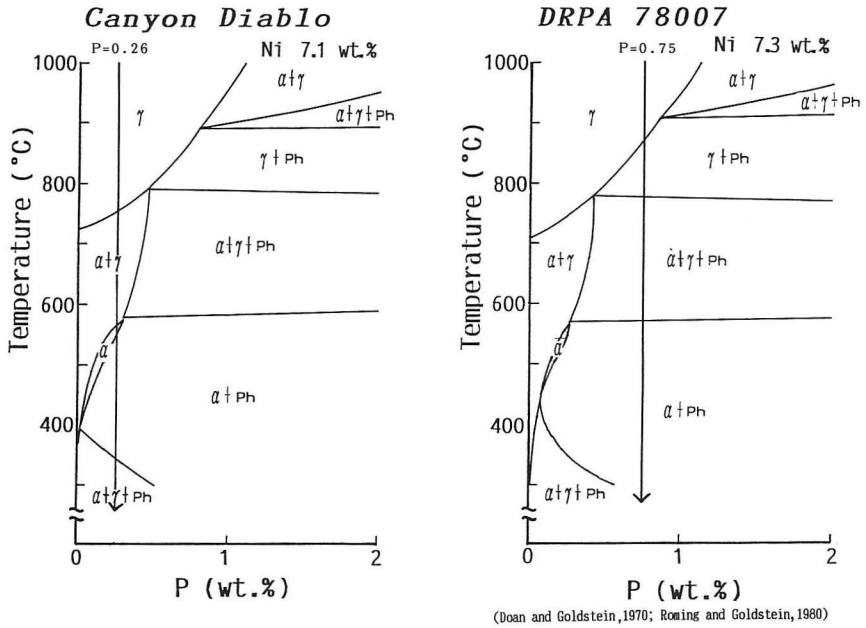


**Text-fig. 10** The phase relationships at each section of bulk Ni content in the Fe-Ni-P system. Arrows show cooling process of Canyon Diablo and DRPA 78007.

partial equilibrium state with metal phase throughout the crystallization. Considering these, it may be possible to discuss the textural changes with crysyallization of schreibersite as follows.

DRPA 78007 shows the textural variations of schreibersite as shown in Plate 1-a & b, 2-d and 3-e. Type(a) schreibersite is bigger in grain size than others, so it may be considered that it has been crystallized at a higher temperature with rapid diffusion rate of P and/or Ni. Ni content of this schreibersite (21.00 atom. %) is lower than that of type(d) schreibersite (39.42 atom. %). Doan & Goldstein (1970) suggests that Ni content of schreibersite coexisting with kamacite increases with a fall of temperature. Therefore, type(a) schreibersite seems to crystallize in higher temperature than type(d) one. Assuming the same cooling rate, it is expected for the idiomorphic schreibersite to crystallize under the low temperature conditions because of its small grain size. Taking into account the phase relationships in the Fe-Ni-P system and the textures of schreibersite mentioned above, the most probable formation process of schreibersite in DRPA 78007 will be summarized as follows. First, xenomorphic and coarse-grained schreibersite (type(a)) crystallizes at about 875℃, and then xenomorphic one crystallizes at about 780℃ in the extension of taenite of a Widmanstätten structure (type(b)) at the $\alpha+\gamma+$Ph field because of grain boundary diffusion. Finally, idiomorphic schreibersite (type(d)) crystallizes at the $\alpha+$Ph field around 570℃.

In case of Canyon Diablo, schreibersite might be crystallized at about 550℃,

where type(a) schreibersite could not be crystallized. Change in chemical composition of schreibersite with textural variations might be less than that of DRPA 78007.

*Compositional change of metal phases during schreibersite crystallization*

In previous chapter, the formation process of schreibersite was discussed only from the viewpoint of bulk composition. Considering the estimated temperature of schreibersite crystallization, change in chemical compositions of metal phases during crystallization of schreibersite is traced on the isothermal sections of P-Ni diagram (Text-fig. 11). The data used for chemical composition (atomic %) and modal proportion(%) of schreibersite in DRPA 78007 are as follows.

Type(a) : 21.0 and 0.8, type(b) : 37.9 and 0.1, and type(d) : 39.4 and 1.5, respectiveiy (Plates 1-3 and Table 3).

Initial bulk contents of both elemtnts are assumed to be on the boundary of $\gamma$ field and $\gamma$+Ph field (solid circle) at 875℃, where type(a) schreibersite might be crystallized. Then bulk Ni and P contents in mctal phases are decreased as shown in the plane at 750℃ (Text-fig. 11) because of the preservation of type(a)

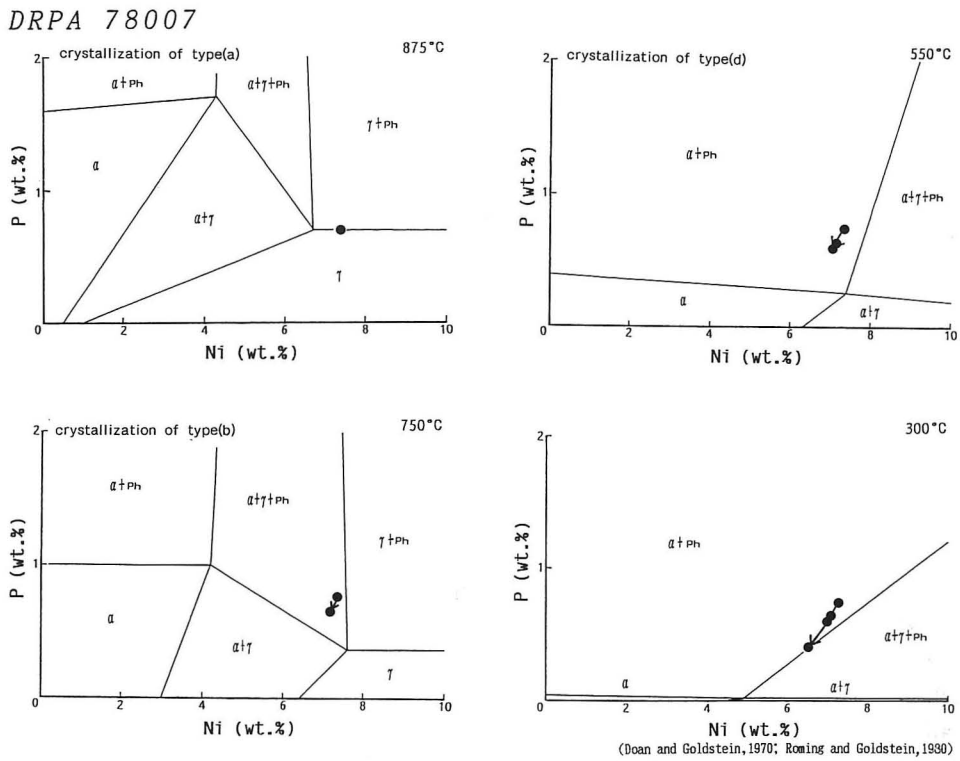


**Text-fig. 11** Stability fields of metal phases and schreibersite in the diagram of P versus Ni (wt. %). Solid circles connected by arrows indicate the change of bulk Ni and P contents in metal phases at each temperature section during cooling of DRPA 78007.

schreibersite. At the plane of 750℃, the changed bulk content in metal phases has been entered $\alpha+\gamma+$Ph field in which type(b) schreibersite could be crystallized. Similar decrease of bulk Ni and P content might be occurred in metal phases as shown in the 550℃ plane of the figure, where it has been enter $\alpha+$Ph field which crystallizes type(d) schreibersite. Further decrease of the bulk contents result in the crystallization of type(e) schreibersite (coexisting with plessite) at 300℃ at the boundary between $\alpha+$Ph and $\alpha+\gamma+$Ph field. As estimated above, it is infered that different types of schreibersite could be crystallized by cooling through the various fields of phase assemblages. Considering the variations in texture and chemical composition, the schreibersite once formed could be removed from the phase equilibrium reaction in the following stages.

Coling rate and estimated size of parent body of iron meteorite

*Cooling rate*

It is possible to discuss the cooling rate of iron meteorite in the parent body on the basis of Ni diffusion rate between kamacite and schreibersite. Cooling rates of iron meteorites have been estimated by many authors at the kamacite and taenite interface (*e. g.* Goldstein, 1968). In this study, it was attempted to obtain the rate at the kamacite and schreibersite interface. Schematic Ni distribution pattern between kamacite and schreibersite is shown in Text-fig. 12, where the Ni contents in kamacite decrease toward the boundary. Cooling rate of iron meteorite is expected to be obtained by reciprocal diffusion equation (Goldstein and Orgilvie, 1965).

Doan and Goldstein (1979) suggest that Ni content of schreibersite increases with falling a temperature. However, Ni diffusion rate becomes slow in kamacite with falling a temperature. As a result, supply of Ni into kamacite-schreibersite interface become insufficient and then Ni gradient is developed in kamacite. Diffusion rate of Ni in chreibersite is more rapid than that in kamacite. Accordingly, the gradient might not be developed in schreibersite. Reciprocal diffusion equation is proposed by Shewmon (1963) as follows.

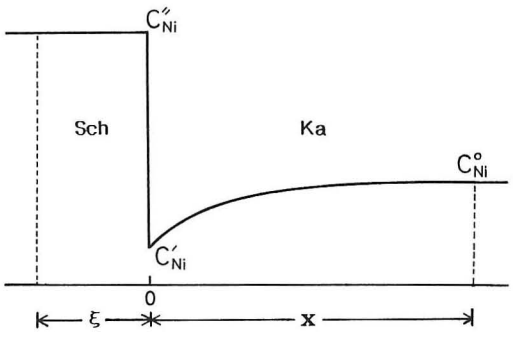


**Text-fig. 12** Schematic distribution pattern of Ni crossing kamacite and schreibersite.

$C_{Ni}(x, t) - C^{\circ}_{Ni} = C'_{Ni} - C^{\circ}_{Ni}\ (1 - \mathrm{erf}(x/2\sqrt{Dt}))$,

where $C_{Ni}(x, t)$ is the Ni content at x frominterface after t second, $C^{\circ}_{Ni}$ is the Ni content of kamacite at sufficiently long distance from interface, $C'_{Ni}$ and $C'_{Ni}$ are the $N_i$ content of kamacite and schreibersite at the interface, $\xi$ is half width of schreibersite, D is the diffusion coefficient of Ni in kamacite and erf is the Gauss' error function.

Simulational conditions and assumuptions are as follows;

1. Diffusion is treatd as one dimensional,
2. Cooling rate is constant,
3. Diffusion coefficient dose not depend upon change in chemical composition,
4. Grain boundary diffusion is neglected.

Based on these assumptions, the cooling rate can be calculated for iron meteorites with elongated type(c) of schreibersite as following procedure, The starting temperature is assumed to be a start of type(c) schreibersite crysntallization based on the Fe-Ni-P phase diagram, while the final temperature is an end of the type(c) one. Next reciprocal diffusion coefficient of Ni in kamacite is used for this calculation.

$D = 3.4 \exp(-58,\ 600/RT)\ (cm^2/s)$ (Uhlig, 1954),

where T is assumed as medium value between starting temperature and final one. P content in kamacite at starting temperature is obtained from Fe-Ni-P phase diagram, while that in schreibersite and kamacite at final temperatures are from analytical data. It does not change in both starting and final temperatures for bulk P content. The unit radius of the crystallization area is obtained by using half width ($\xi$) and Ni content ($C''_{Ni}$) of single schreibersite for determination of its diffusion field length, which is considered to be a distance from interface (X). Analytical data of kamacite are available for $C_{Ni}(x, t)$ ($=C^{\circ}_{Ni}$) and $C'_{Ni}$ in the equation.

Obtained time (t: sec.) from the diffusion equation (Shewmon, 1963) is used for calculation of cooling rate between starting and final temperatures of the type(c) schreibersite crystallization. The calculated rates for four iron meteorites are shown in Table 7. The estimated cooling rate of Canyon Diablo in $1.1 \times 10^6$ (year/°C), while Odessa is $1.7 \times 10^6$ (year/°C). The cooling rate obtained from kamacite-taenite interface (Goldstein, 1968) is also shown in the same table. The rate from kamacite-schreibersite tends to show more rapid than that from kamacite-taenite, but these two results are not so different in order. In another, that of ALH-77263 and North Chile are $8.7 \times 10^7$ (year/°C) and $2.3 \times 10^6$ (year/°C), respectively. In summarizing the result obtained, cooling rate of Canyon Diablo, Odessa and North Chile are $10^6$ (year/°C) in order, while ALH-77263 shows slower rate about two unit in order than the others.

The relationships between Ni partition relationships and cooling rate in Canyon Diablo, North Chile and ALH-77263 are shown in Text-fig.6 and Table 7. It is

**Table 7** Calculated cooling rates of iron meteorites.

| | Canyon Diablo | Odessa | ALH-77263 | North Chile |
|---|---|---|---|---|
| Ni content in Schreibersite (wt. %) | 37.99 | 31.02 | 31.12 | 28.48 |
| Ni content in Kamacite (wt. %) | 6.17 | 6.58 | 5.89 | 5.19 |
| P content in Kamacite (wt. %) | 0.06 | 0.08 | 0.09 | 0.04 |
| half width of Schreibersite ($\mu$m) | 20 | 40 | 28 | 35 |
| Starting temperature (℃) | 550 | 550 | 500 | 550 |
| Final temperature (℃) | 350 | 370 | 320 | 300 |
| Cooling rate (yr./℃) | $1.1\times10^{6}$ | $1.7\times10^{6}$ | $8.7\times10^{7}$ | $2.3\times10^{6}$ |
| Cooling rate (Goldstein, 1968) | $2.5\times10^{6}$ | $3.0\times10^{6}$ | | |

observed that chemical composition of schreibersite changes with textural variations in Canyon Diablo and North Chile. But that of schreibersite does not show intimate relationships with texture so much in ALH-77263. ALH-77263 shows slower cooling rate than Canyon Diablo and North Chile among these three samples. It is deduced that ALH-77263 had been cooled with more equilibrated state depending on slower cooling than another samples.

*Size of parent body*

As estimated above, cooling rates of iron meteorites are individually different from among the samples. It will be discussed here on the size of parent bodies of iron meteorires on the basis of their cooling rates. Thermal conduction with a spherical body is represented by the next equation (Williamson and Adams, 1919).

$$\frac{T-T_S}{T_0-T_S}=\frac{2}{\pi}\sum_{n=1}^{\infty}\frac{\frac{R}{r}\sin\frac{n\pi r}{R}}{n\cdot(-1)^{n+1}}e^{(\kappa n^2\pi^2/R^2)\cdot t},$$

where the abbreviations are as follows; Ts: the surface temperature (°C), To: the initial homogeneous temperature (°C), R: the radius of the sphere (cm), r: the distance from the center (cm), $\kappa$: the thermal conductivity ($cm^2$/sec), t: the time (sec).

The following conditions are assumed in the calculation: Iron meteorite forms a core of parent body, and is covered with chondritic material. Thermal conductivity of chondritic material is $4.7\times10^{-3}$ ($cm^2$/sec) by Begemann *et al.* (1969). In assumption of simple cooling, homogeneous temperature in its early stage is 1000°C, and the temperature in surface of the parent body is 0°C (Begemann *et al.*, 1969). The temperature changes in a core of parent body with a different radius was calculated as shown in Text-fig. 13. It shows that the temperature of core does not

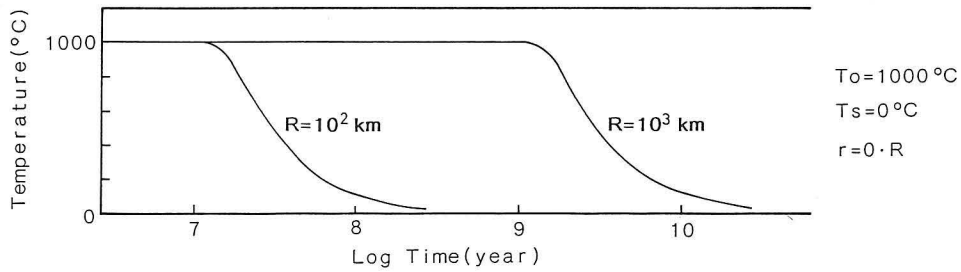


**Text-fig. 13** Estimated temperature changes in a core of parent astrobody with a different radius.

change until certain time and after then it begins to fall. The beginning time to fall the temperature is getting slower with increase of radius of parent body. Namely, the bigger parent body in radius takes the longer cooling time.

The radius of parent body is calculated for Canyon Diablo, Odessa, ALH-77263 and North Chile from the cooling rate and a equation of thermal conduction. Table 7 represents temperature ranges of calculated cooling rate which are applied to the equation for thermal conduction. The obtained radii of parent body for each meteorite are described in Table 8. The estimated radii of parent body are about 270 km for Canyon Diablo and 2,350 km for ALH-78252.

In the discussion for the difference of cooling rate, we have to pay attention to the dependence not only upon the radius of parent body but also upon the original site of meteorite in the interior of the parent body.

Equilibrium state of iron meteorite

It is recognized that the texture of schreibersite is individually different in thirteen iron meteorites used in this study. Some iron meteorites show a textural variety of schreibersite in the same sample, and another only single texture. On the other hand, chemical composition of schreibersite is also different even in the same specimen in some cases. One show a wide range of chemical composition

**Table 8.** Estimated radii of parent bodies of iron meteorites.

| Name | Cooling rate(yr./℃) | Radius of parent body(km) |
|---|---|---|
| Canyon Diablo | $1.1\times10^{6}$ | 270 |
| Odessa | $1.7\times10^{6}$ | 340 |
| ALH-77263 | $8.7\times10^{7}$ | 2350 |
| North Chile | $2.3\times10^{6}$ | 380 |

**Explanation of Plate 1**

Photomicrographs of schreibersite: (a) xenomorphic and coarse-grained schreibersite coexisting with kamacite, (b) xenomorphic schreibersite in the extension of taenite with the Widmanstätten structure. Ni contents (atom. %) of schreibersite are shown for DRPA 78007.

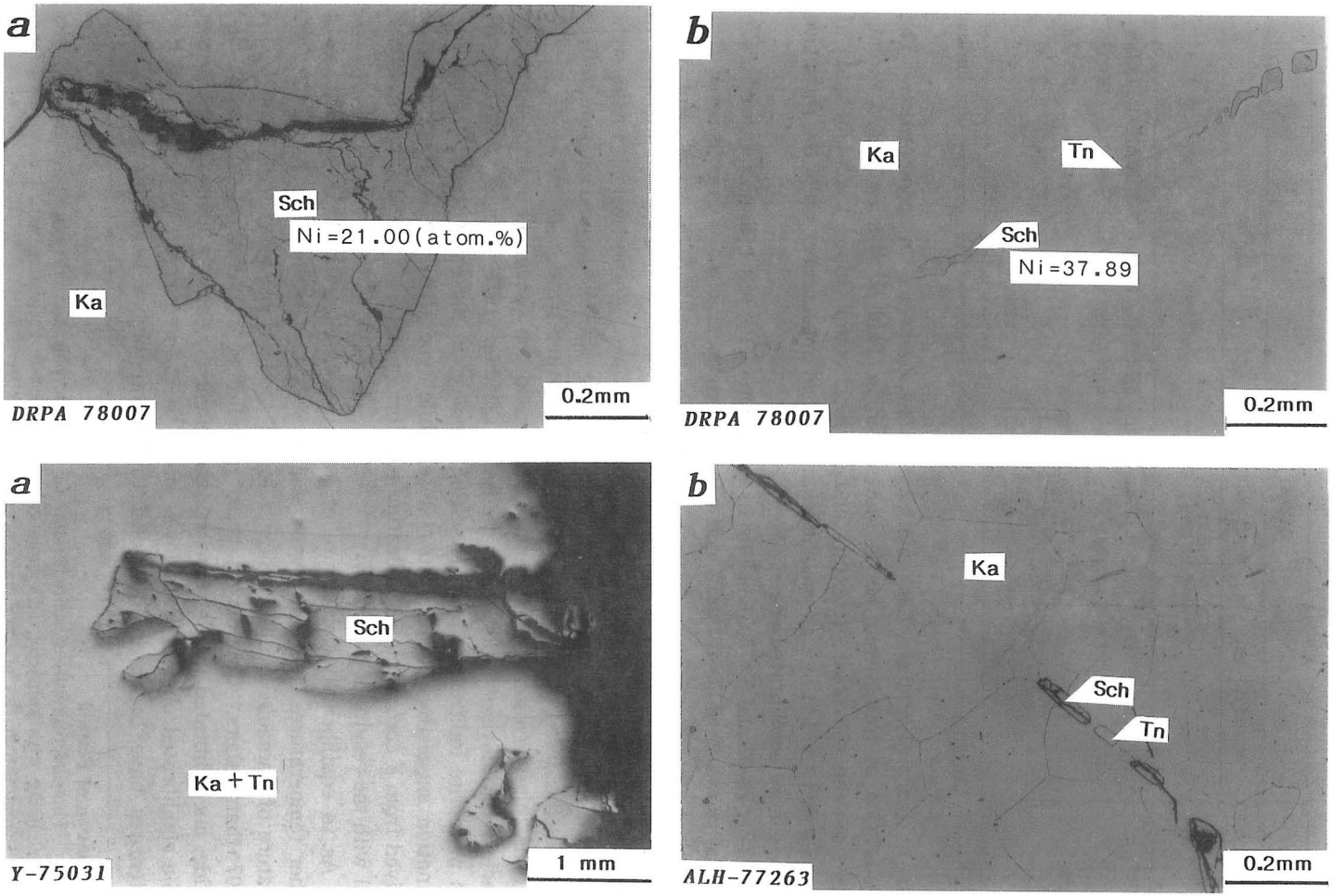


Sch : Schreibersite Ka : Kamacite Tn : Taenite

**Table 9** Classification of iron meteorites basced on the texture and the chemical composition of schreibersite.

| Texture | multiple | | | single |
|---|---|---|---|---|
| Composition | heterogeneous | intermediate | homogeneous | |
| Colling rate (yr./℃) | | $1.1\times10^{6}$~$2.3\times10^{6}$ | $8.7\times10^{7}$ | |
| Name | DRPA 78007 IIB Ogg<br>Y-75031 ? Opl | Canyon Diablo IA Og<br>Odessa IA Og<br>ALH-77283 IA Og<br>Harlowton IA Om<br>North Chile II AH | ALH-77263 IA Og<br>ALH-78252 IVA Om | Y-790517 IIIA Om<br>Y-790724 IIIA Om<br>Boxhole IIIA Om<br>Y-791694 ? D |

Unequilibrium ←——————————→ Equilibrium

with a textural change, but another is homogeneous in composition. The classification of iron meteorites is represented in Table 9 with estimated cooling rates from the viewpoint of texture and chemical composition of schreibersite. It indicates that the left side is unequilibrium state in appearance, while the right side becomes more equilibrated one.

DRPA 78007 and Y-75031 belong to the group of the left column. Schreibersite in them shows variable textures and chemical compositions. it is considered that these iron meteorites are formed under the unequilibrium state. But each schreibersite with different texture is assumed to maintain a local equilibrium with kamacite in them. Y-790517, Y-790724, Boxhole and Y-791694 belong to the right column. Schreibersite shows only single texture with homogeneous composition which is considered to be formed under the equilibrium state.

The classification by Wasson (1974) based on chemical compositions is attached to individual meteorite. Kelly & Larimer (1977) suggest that type IA iron meteorite indicates a partial melting products in the early stage of planetary formation suggesting unequilibrium state, while type IIIA one is assumed to be derived from a core of planet indicating equilibrium state. These estimations agree well with the results of this study.

As to equilibrium temperature of kamacite-taenite, DRPA 78007 indicates a higher temperatures than Harlowton and Y-790724. On the other hand, the temperature of kamacite-troilite indicates higher temperature for Y-75031 and DRPA 78007 than others. Considering these equilibrium temperatures of metals and sulfide, unequilibrated iron meteorites tend to show relatively higher temperatures, while equilibrated ones indicate lower ones. It is infered that unequilibrated iron meteorites have been rapidly cooled to indicate higher temperature conditions,

**Explanation of Plate 2**

Photomicrographs of schreibersite: (c) xenomorphic and fine-graind schreibersite coexisting with kamacite, (d) idiomorphic schreibersite coexisting with kamacite. Ni content (atom. %) of screibersite is shown for DRPA 78007.

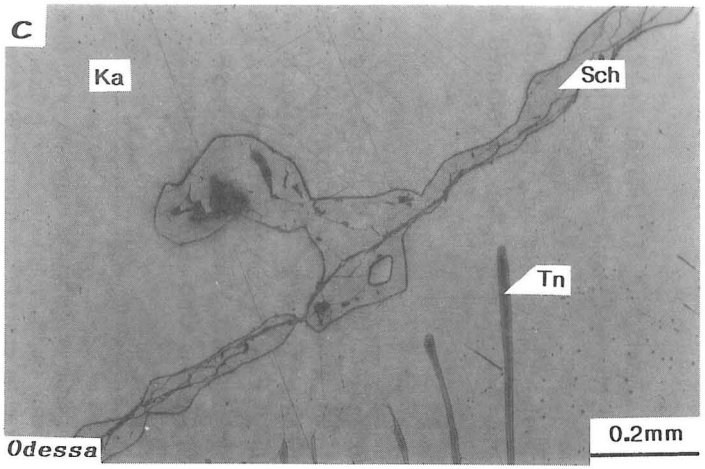


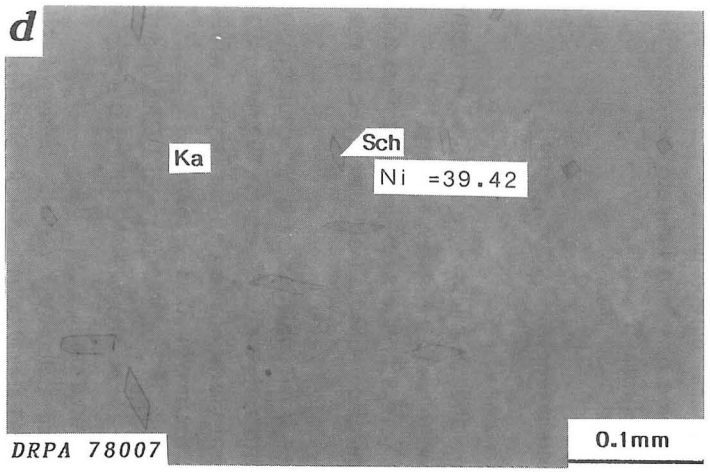


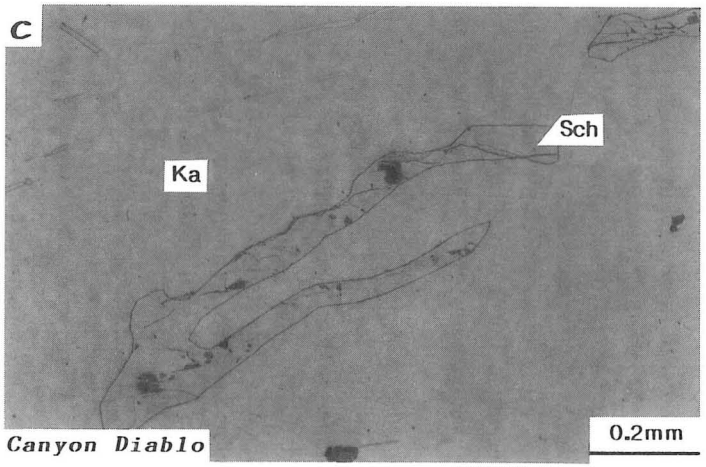


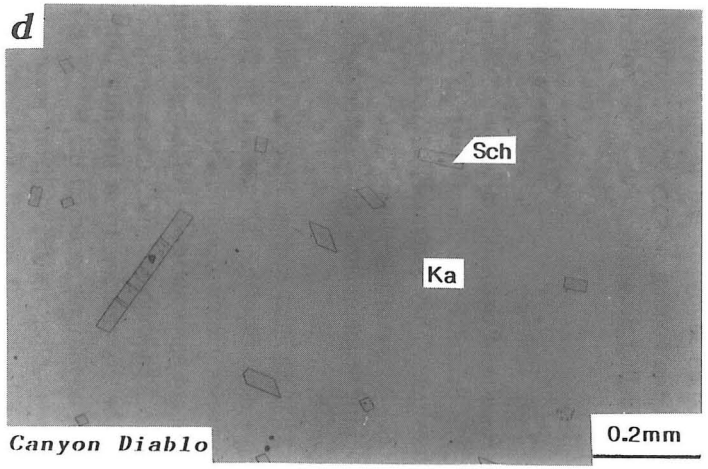


Sch : Schreibersite Ka : Kamacite Tn : Taenite

Plate 2

while equilibrated ones slowly to maintain the diffusion till the lower temperatures.

Detailed study of the texture and the chemical composition of schreibersite clarified the cooling history of iron meteorites some of which indicate the unequilibrium cooling processes as a whole with local equilibrium.

## Summary and conclusions

Results of this study are summarized as follows;

1) Schreibersite shows variable textures and chemical compositions in iron meteorites. They are classified into seven types based on those variations.

2) Ni variations from 20 to 40 atomic % in schreibersite are recognized not only in iron meteorites with varied bulk chemical composition but also even in one specimen.

3) Chemical composition of schreibersite is strongly affected by equilibrium temperature in which Ni content increases with falling temperature. Schreibersite changes its chemical composition with texutural variations in Canyon Diablo, while it does not show intimate relationships with a texture in ALH-77263.

4) Xenomorphic and coarse-grained schreibersite in Y-75031 and DRPA 78007 might be crystallized from stability field of $\gamma$+Ph at about 800°C under the rapid cooling conditions based on the Fe-Ni-P phase diagram.

5) Cooling rates of iron meteorites were calculated on the basis of Ni diffusion between kamacite and schreibersite. ALH-77263 indicates $8.7\times10^{7}$(year/°C), while Canyon Diablo, Odessa and North Chile $10^{6}$ in order. ALH-77263 might be cooled with more equilibrated state than others.

6) Relatively larger size of parent body is estimated for ALH-77263 (r=2,350 km) compared with Canyon Diablo, Odessa and North Chile (r=270-380 km) on the basis of cooling rate.

7) Textural and compositional variations of schreibersites are interpreted by different cooling rate and process of iron meteorites, in which they maintained a local equilicrium with coexisting metal phases.

*Acknowledgements*

We are very grateful to Professor Shunzo Yui of Hokkaido University for his guidance and critical reading of manuscript. We would like to acknowledge the kind advice and valuable discussion of Associate Professor Takeshi Kikuchi of Hokkaido University. We are also much indebted to Mr. Shoichi Terada for his support of EPMA analyses. Associate Professor Keizo Yanai and Dr. Hideyasu Kojima of National Institute of Polar Research gave us kind support and advice.

---

**Explanation of Plate 3**

Photomicrographs of schreibersite: (e) xenomorphic schreibersite coexisting with plessite, (f) xenomorphic schreibersite coexisting with troilite, sphalerite (or cohenite), (g) platy schreibersite. Ni content (atom. %) of schreibersite is shown for in DRPA 78007.

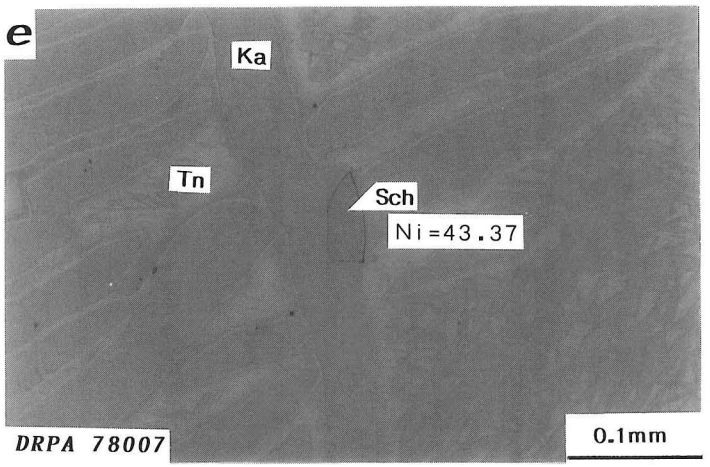


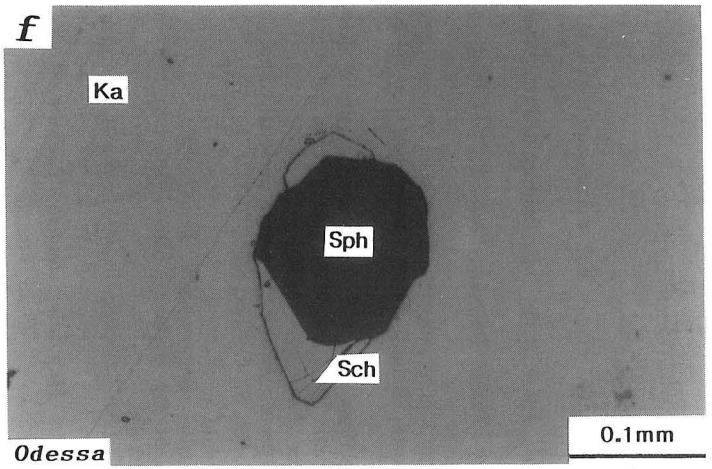


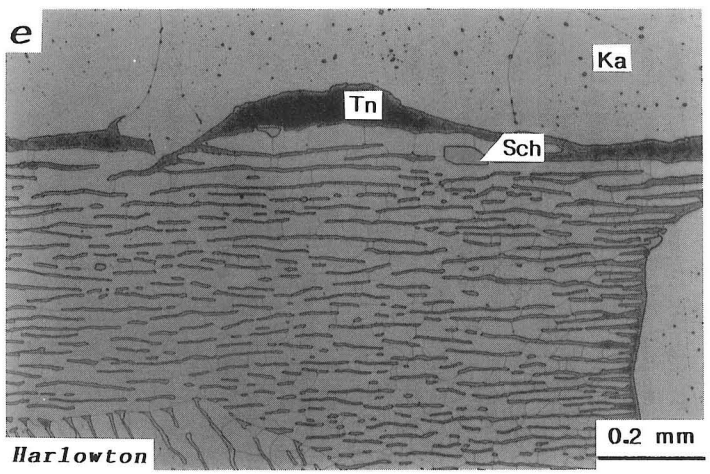


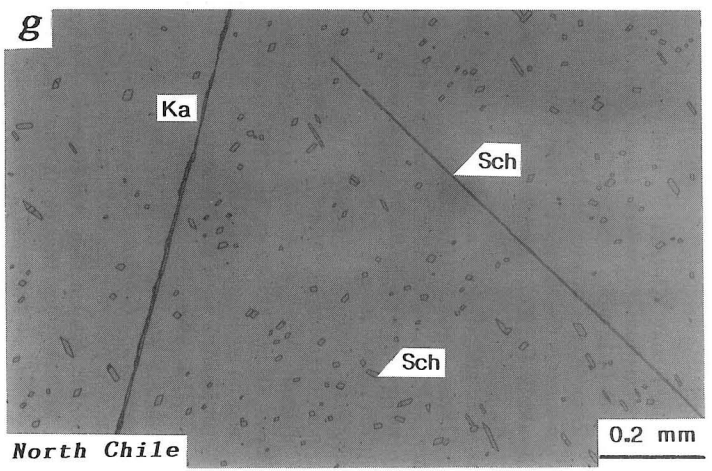


Sch : Schreibersite Ka : Kamacite Tn : Taenite Sph : Sphalerite

## *References*

Begemann, F. and Wlotzka, F., 1969. Shock induced thermal metamorphism and mechanical deformations. *Geochim. Cosmochim. Acta*, 33 : 1351-1370.

Bezmen, N. I., Lyutov, V. S. and Osadchii, E. G., 1978. Raspedelenie nikelya mjdu troilitom i metallicheskim jellzom kak mineralogicheakii termometr. *Geohimiya*, 10 : 1466-1473.

Buchwald, V. F., 1975. *Handbook of iron meteorites, Vol. 1, 2, 3.* Univ. California Press, 1418 pp.

Doas, A. S. and Goldstein, J. I., 1970. The Ternary Phase Diagram, Fe-Ni-P. *Metallurgical Transactions*, 1 : 1759-1767.

Fisher, R. M., Spangler, C. E. Jr. and Nagata, T., 1978. Metallographic properties of Yamato iron meteorite, Yamato 75031 and stony-iron meteorite, Yamato 74004. *Mem. Natl Inst. Polar Res., Spec. Issue*, 8 : 248-259.

Fisher, R. M., Szirmal, A. and Nagata, T., 1980. Metallographic and magnetic properties of Antarctic meteorites, Allan Hills-77255, Derrick Peak-78003 and-78007, and Russian meteorite, Sikhote-Alin. *Mem. Natl Inst. Polar Res., Spec. Issue*, 17 : 276-290.

Fujikawa, O. and Matsueda, H., 1991. Digital image processing system using a personal computer and its applications. *Jour. Japan. Assoc. Min. Pet. Econ. Geol.*, 86 : 346-353. (in Japinese with English abstract)

Goldstein, J. I., 1968. The classification of iron meteorites. *Meteorite Res.*, 59 : 721-737.

Goldstein, J. I. and Ogilvie, R. E., 1965. The growth of the Widmanstatten Pattern in Metallo Meteorite. *Geochim. Cosmochim. Acta*, 29 : 893-920.

Graham, A. L., Bevan, A. W. R. and Hutchison, R., 1985. *Catalogue of Meteorites*, London, British Museum (Natural History), 460 pp.

Hirata, M., 1985. Quantitative X-ray microanalysis. in *Microbeam Analysis*. Asakura-Shoten : 222-230. (in Japanese)

Kelly, W. R. and Larimer, J. W., 1977. Chemical fractionations in meteorite-VIII. Iron meteorites and the cosmochemical history of the metal phase. *Geochim. Cosmochim. Acta*, 41 : 93-111.

Nagata, T., Funaki, M. and Taguchi, I., 1984. Magnetic analysis of new Antarctic iron meteorite. *Mem. Natl Inst. Polar Res., Spec. Issue*, 35 : 302-318.

Nagata, T., Masuda, A. and Taguchi, I., 1983. Chemical studies on the Antarctic iron meteorites, Yamato-790724, ALH-77263 and ALH-77289. *Mem. Natl Inst. Polar Res., Spec. Issue*, 30 : 237-245.

Nagata, T., Masuda, M., Taguchi, I. and Ono, Y., 1986. Chemical study on the distribution of germanium and gallium in Antarctic iron meteorites. *Mem. Natl Inst. Polar Res., Spec. Issue*, 42 : 287-296.

Reed, S. J. B., 1975. *Electron Microprobe Analysis*, Cambridge University Press, 400 pp.

Roming, A. D., Jr. and Goldstein, J. I., 1980. Determination of the Fe-Ni and Fe-Ni-P phase diagrams at low temperatures (700℃-300℃). *Meoallurgical Transactions Acta*, 11A : 1759-1767.

Shewmon, P. G., 1979. *Diffusion in Solids*. McGraw-Hill Book Company.

Uhlig, H. H., 1954. Contribution of metallurgy to the study of meteorite. Part 1-structure of metallic meteorites, their composition and the effect of pressure. *Geochim. Cosmochim. Acta*, 6 : 282-301.

Wasson, J. T., 1974. *Meteorite : Classification and Properties*. New York, Springer-Verlag, 316 pp.

Williamson, E. D. and Adams, L. H., 1919. Temperature distribution in solids during heating or cooling. *Phys. Rev.* 14 : 99-114.

(Manuscript received on June 4, 1992 ; and accepted on June 29, 1992)